Determining laser-induced dissociation pathways of multielectron diatomic molecules: Application to the dissociation of O_2^+ by high-intensity ultrashort pulses

A. M. Sayler, P. Q. Wang, K. D. Carnes, B. D. Esry, and I. Ben-Itzhak
J. R. Macdonald Laboratory, Department of Physics, Kansas State University, Manhattan, Kansas 66506, USA
(Received 8 July 2006; revised manuscript received 9 March 2007; published 25 June 2007)

A method for determining the laser-induced dissociation pathways of multielectron diatomic molecules is developed. Despite the abundance of possible dissociation pathways inherent to such molecules, this technique allows one to resolve the dissociation pathways that contribute to the measured intensity-dependent three-dimensional momentum distribution. To illustrate this method, the unique dissociation mechanisms and pathways producing a few predominant features in the laser-induced dissociation momentum distribution of O_2^+ are determined.

DOI: 10.1103/PhysRevA.75.063420 PACS number(s): 33.80.Wz, 42.50.Hz

I. INTRODUCTION

There is a great deal of ongoing theoretical and experimental work concerned with understanding the dynamics of diatomic molecules in intense short pulse laser fields. However, interpretation of the experimental results for multielectron molecules has been crude compared to the extensive theoretical and experimental studies of H_2-laser interactions discussed in several excellent papers and reviews [1–26]. This is mainly due to the more complex electronic structure of multielectron diatomic molecules as is evident in Fig. 1 for O_2^+. The abundant work with H_2 has given rise to a conceptual understanding of molecular dissociation in terms of the Floquet picture. Others have used parts of this picture to reduce the number of possible electronic states involved in the laser-induced ionization and dissociation of multielectron molecules. For example, Hishikawa *et al.* used angular distributions to limit possible dissociation pathways [27], and Alnaser *et al.* used kinetic energy release (KER) to find initial and final states in double ionization [28]. Taking this one step further, by combining all the information given by the Floquet picture with a complete intensity-dependent three-dimensional (3D) momentum imaging technique, we suggest a method to uniquely determine the laser-induced dissociation pathways of a multielectron diatomic molecule.

In the diabatic Floquet representation, which gives diabatic field-dressed potential energy curves, the emission or absorption of n photons corresponds to the shifting of the potential energy curves (PECs) up or down by the energy of n photons (i.e., $\pm n\hbar\omega$), respectively, where the shifted states are denoted by the state followed by $\pm n\omega$. For example, $2p\sigma_u - 1\omega$ is the $2p\sigma_u$ state with absorption of one photon. After the initial curves are duplicated in this way, the dissociating nuclear wave packet can make a transition at any crossing that obeys the molecular dipole selection rules. Furthermore, the transition probability at each crossing is proportional to the absolute square of the dipole matrix element. In contrast to the diabatic Floquet picture, which is most appropriate for laser intensities in the perturbative regime, the adiabatic Floquet representation is best suited for laser fields beyond the perturbative regime. However, one can still use the diabatic representation for intense laser pulses by including the effect of the laser field strength in the coupling terms between these states. For example, this scheme was used successfully to interpret the dissociation of Na_2^+ by both experimentalists [30] and theorists [31]. Furthermore, this simplified representation helps one quickly explore possible dissociation pathways without the additional calculations needed to generate the adiabatic potential curves for each laser intensity.

As seen in Fig. 2(a), the small number of effective PECs in H_2^+ allows one to interpret the adiabatic Floquet picture rather easily, thus giving rise to the concepts of bond softening, vibrational trapping (also called bond hardening), and above-threshold dissociation [6–9]. In contrast to the relatively simple picture for H_2^+, multielectron diatomic molecules such as O_2^+ create a diabatic Floquet picture with a plethora of PEC crossings, allowing for a multitude of laser-induced dissociation pathways, referred to simply as pathways below. A discussion of the interactions of a variety of "small" molecules, in particular diatomic, with intense laser fields is found in the detailed reviews by Codling and Frasinski [32], as well as Posthumus [9], and references therein. The behavior of the oxygen molecule in intense laser fields, in particular, has been widely studied for many years (see, for example, Refs. [27,28,32–45]). More specifically, these studies of the dissociative ionization of O_2 spanned a variety of wavelengths, pulse durations, and intensities along with

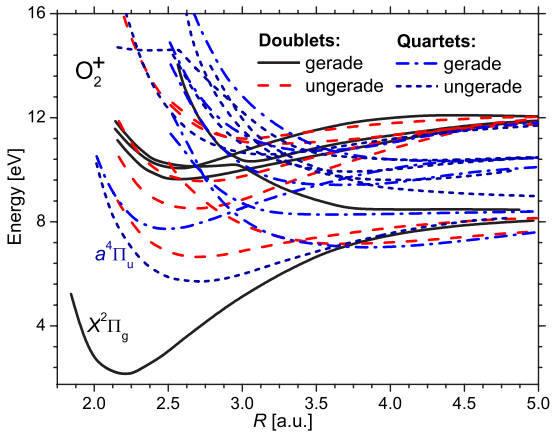

FIG. 1. (Color online) O_2^+ Born-Oppenheimer PECs [29]. The doublet and quartet states are separated into gerade and ungerade groups and the two possible initial electronic states in this experiment, $X\,^2\Pi_g$ and $a\,^4\Pi_u$, are labeled.

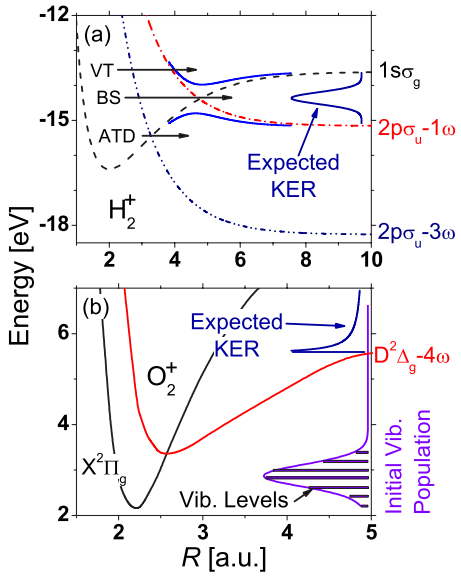

FIG. 2. (Color online) (a) A schematic Floquet picture of the H_2^+ diabatic PECs with adiabatic PECs superimposed at the one-photon crossing (solid lines) for $\lambda \sim 790$ nm. The processes of bond softening (BS), vibrational trapping (VT), and above-threshold dissociation (ATD) are depicted. (b) The initial vibrational distribution of the O_2^+ doublet ground state and a possible dissociation pathway discussed in the text. The expected KER distributions for the $X\,^2\Pi_g \rightarrow D\,^2\Delta_g - 4\omega$ and BS pathways are displayed in (b) and (a), respectively. Note that only the relative heights in these distributions are meaningful.

various levels of ionization. However, unambiguous determination of the dissociation pathways using a picture as elegantly simple as the H_2^+ Floquet picture has been absent until recently. Recent kinematically complete studies of the dissociation into $O^+ + O^+$ following double ionization had sufficient resolution to identify the transient electronic state of O_2^+ [28].

In this work, we utilize an O_2^+ beam target and coincidence three-dimensional momentum imaging to perform measurements with similar resolution for the dissociation of O_2^+ into $O^+ + O$ without the need for the laser to first ionize the target. Furthermore, we use what is known about the dynamics of H_2^+ in intense laser fields, where nonperturbative behavior dominates, as a foundation for determining the most probable dissociation pathways of O_2^+ from the measured intensity-dependent momentum distribution of the dissociation fragments. The abundance of photodissociation pathways in the diabatic Floquet picture of O_2^+ may make this task seem insurmountable. However, by evaluating the dissociation distribution, most, if not all, noncontributing pathways can be eliminated. This is accomplished using four conditions outlined here and discussed in detail momentarily. First, the intensity at which a dissociation feature is predominant, I_{pred}, is related to the sum of absorbed and emitted photons, n, required along the pathway, i.e., higher n corresponds to higher I_{pred}. Second, the shape and position of the KER peak generated by a particular pathway is influenced by the shape of the PECs comprising it. Third, the number of transitions favoring internuclear alignment parallel and perpendicular to the laser polarization required along a pathway will determine the angular distribution of the channel. Fourth, all transitions involved in a pathway must obey the molecular dipole selection rules. In addition, we assume that all dipole matrix elements for the relevant allowed transitions are of comparable magnitude.

II. EXPERIMENTAL METHOD

Using an 8 keV O_2^+ ion beam produced in an electron cyclotron resonance (ECR) ion source and a coincidence 3D momentum imaging technique, we performed kinematically complete measurements of the laser-induced dissociation of an O_2^+ target. The O_2^+ molecular ions are formed by electron impact ionization in the ion source. This process produces an O_2^+ beam that is predominantly in the $X\,^2\Pi_g$ and $a\,^4\Pi_u$ electronic states, the former comprising about $2/3$ and the latter about $1/3$ of the beam [46]. $X\,^2\Pi_g$ is the electronic ground state of O_2^+, and $a\,^4\Pi_u$ is metastable and the lowest-lying quartet state. For the sake of brevity, only the dissociation of O_2^+ at intensities up to 10^{15} W/cm^2 will be discussed here.

Under the conditions of this study, dissociation of highly excited vibrational states of O_2^+ plays an important role. The lowest electronic states in both the doublet and quartet manifolds of this molecular ion have a broad vibrational population. Typically, molecular ions produced by electron impact ionization in an ion source have a population distribution roughly determined by the Franck-Condon factors (see, for example, [47] for the population of H_2^+). Deviations from the Franck-Condon distribution can occur, especially when ionization of higher electronic states, which feed the lower state by cascades, are significant. This is the case for the $a\,^4\Pi_u$ state of O_2^+ [48]. However, the resulting vibrational population is still broad and falls off for the highest vibrational states. Furthermore, it is important to note that in the upcoming interpretation of the dissociation data, the only relevant facts are that high vibrational states of O_2^+ have significant population and that the population of these states, particularly for the doublet, falls off for very high vibrational states.

The laser beam, which is provided by a Ti:sapphire chirped-pulse amplification laser system with a central wavelength of 790 nm, a Fourier-transform-limited pulse duration of 35 fs [full width at half maximum (FWHM) in intensity], a 1 kHz repetition rate, and a pulse energy of about 1 mJ, is stretched to 40 ± 5 fs by introducing a positive chirp. The linearly polarized pulse, which is focused by an $f = 200$ mm lens, is incident upon the center of the ion beam, and the laser polarization, laser propagation, and ion beam are normal to one another. The fragments from the dissociation, O^+ and O, are separated in time by the constant weak electric field of a spectrometer in the ion beam direction and are detected by a time- and position-sensitive microchannel-plate delay-line detector, which records time and position information for all fragments created in each laser pulse. This time and position information allows for the reconstruction of the initial 3D momenta of the O^+ and O fragments. True dissociation events are distinguished since both fragments, O^+ and O, are recorded in coincidence with a particular laser pulse. In addition, we require that momentum is

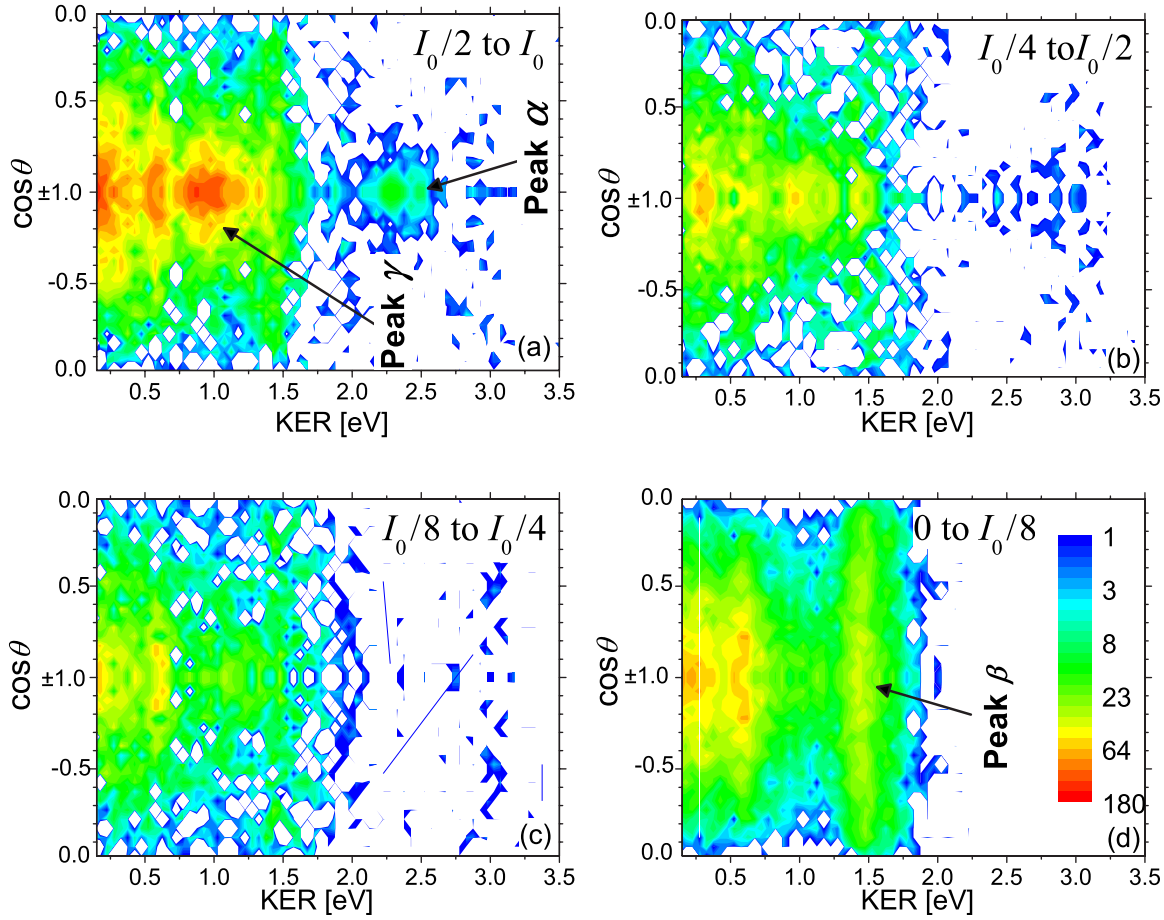

FIG. 3. (Color online) Experimental data for the dissociation of O_2^+ in a 40±5 fs 790 nm laser field, where $I_0=(1.3\pm0.5)\times10^{15}$ W/cm^2 and θ is the angle between the laser polarization and the internuclear axis of O_2^+. (a)–(d) The contributions of four different intensity slices, which comprise the total ion-laser interaction volume, as a function of KER and cos θ.

conserved, as the absorbed and emitted photons have negligible momenta compared to the dissociating nuclei. A detailed description of this apparatus and technique is given in previous publications [49–51].

The contributions to the total dissociation distribution that come from a particular intensity range within the laser-molecular ion interaction volume are distinguished using the intensity difference spectrum (IDS) method [52], which is applicable because our ion beam width is much smaller than the Rayleigh range and much larger than the laser waist [53]. The IDS method allows one to subtract contributions from the low intensity wings of the laser spatial distribution, and thus determine the effects of a given intensity range or slice (see Refs. [52,50] for details). Conducting a sequence of such differential measurements in intensity allows one to examine a feature's behavior in these successive intensity slices, therefore providing the intensity dependence of that feature. We plot these distributions as a function of KER and cos θ, where θ is the angle between the laser polarization and the internuclear axis of the O_2^+ being interrogated by the laser. In the following interpretation of the measured angular distributions we assume that the O_2^+ molecular ions are randomly aligned and that the axial-recoil approximation [54,55] is valid. Namely, we assume that alignment effects are negligible both during and after the laser pulse. It has been recently shown that postionization alignment modifies the angular distribution in double ionization of O_2 if the intense laser pulse is not sufficiently short [45]. However, one would expect this phenomenon to be less important for O_2^+ dissociation in our measurements because the number of photons exchanged with the laser field is much smaller than in double ionization of O_2, therefore causing on average a smaller angular momentum transfer.

III. RESULTS AND DISCUSSION

A. Determining laser-induced dissociation pathways

As one can see from the intensity-dependent KER-cos θ distributions in Fig. 3, the rich electronic structure of O_2^+ produces numerous distinct features [56], which give us insight into the pathways. Although the number of electronic states in O_2^+ is formidable, the intensity-dependent laser-induced dissociation distributions provide three pieces of information about the pathway of a particular channel.

First, since the IDS method allows one to determine at what intensity each feature is predominant, one can narrow down the possible number of photons and transitions involved in a particular pathway. In general, features appearing at higher intensities require more photons than those appear-

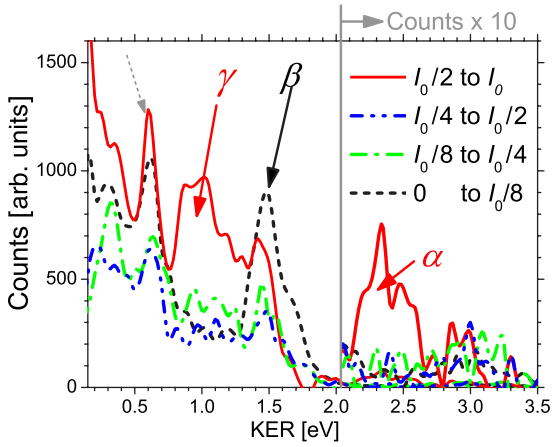

FIG. 4. (Color online) The measured KER distributions of O_2^+ dissociation for the same four intensity slices shown in Fig. 3 integrated over cos θ. Lines indicate splines through the data points and the dissociation pathways yielding the KER peaks labeled as α, β, and γ are discussed in the text.

ing at lower intensities. Furthermore, if one can determine the pathway for any feature, that feature can then be used as an intensity benchmark for other features. For example, if (i) there are two features labeled δ and ε, which appear at intensities I_δ and I_ε, respectively, (ii) δ is known to correspond to a pathway requiring three photons, and (iii) $I_\varepsilon < I_\delta$, then the pathway leading to ε requires three or less photons. In this way, lower and upper bounds can be placed on the number of photons involved in the pathway leading to a feature by the identification of other features.

Second, the position and shape of the KER distribution for each peak, as seen in Fig. 4, allows one to determine the height and general shape of the barrier over which the vibrational wave packet dissociates. This can easily be seen in the contrast between the expected KER distributions from the curves displayed in Figs. 2(a) and 2(b). The BS pathway in H_2^+ will produce a KER distribution peaking around 0.8 eV as that is the position of the diabatic Floquet curve crossing above the $2p\sigma_u - 1\omega$ dissociation limit. The width of the KER peak should correspond to the gap between the adiabatic curves weighted by the vibrational population. In contrast, the O_2^+ PECs, shown in Fig. 2(b), will produce a KER distribution peaked at 0 eV that dies off exponentially with KER. This is because the $D\,^2\Delta_g - 4\omega$ dissociation limit is above the PEC crossing and the vibrational distribution of $X\,^2\Pi_g$ tails off exponentially at this point.

Third, the angular distribution of a particular feature points to the number and type of transitions involved in its pathway by way of the angular momentum quantum number Λ. Each transition from one potential curve to another can be classified as either a parallel transition ($\Delta\Lambda = 0$), which depends on the laser field strength parallel to the internuclear axis, or a perpendicular transition ($\Delta\Lambda = \pm 1$), which depends on the laser field perpendicular to the O_2^+ axis. Furthermore, only different pathways that begin and end on the same PECs can interfere. Therefore, pathways with unique ending and/or starting points can be treated incoherently. The vast majority of O_2^+ pathways fall under the latter case. Thus, one would expect a solitary KER-cos θ feature produced by a single pathway to have a $\cos^{2n}\theta \sin^{2m}\theta$ distribution, where n and m are the number of photons emitted and absorbed in parallel and perpendicular transitions along the pathway, respectively [27].

In addition to these three constraints imposed by the data, molecular dipole transition selection rules for homonuclear molecules apply, thus allowing us to further weed out ineffectual crossings and determine the most likely pathway. In a laser field, doublet and quartet states only interact with other doublet and quartet states, respectively. Thus, the set of all O_2^+ electronic states, which consists of doublet and quartet states, can be separated into two mutually exclusive sets. Furthermore, only transitions that obey dipole selection rules are allowed. Thus, for an n-photon transition, if n is odd, the transition must be gerade (g) to ungerade (u) or u to g, and if n is even, the transition must be g to g or u to u.

B. Examples

1. Peak α

To illustrate this procedure, we will detail the determination of pathways that lead to two distinct KER-cos θ features, α and β as denoted in Figs. 3 and 4. The most distinct feature of channel α is its sharp peak around the laser polarization, as seen in Fig. 5(a). This peak is best fit by a $\cos^{2n}\theta$ function if $n=3$. Therefore, after implementation of the aforementioned transition rules, the pathway can be assumed to have only parallel transitions, as any perpendicular transitions along the pathway would create an angular distribution greatly different from the one measured. Thus, the pathway must consist of $X\,^2\Pi_g$ followed by $^2\Pi$ states or $a\,^4\Pi_u$ followed by $^4\Pi$ states, provided that the axial-recoil approximation is valid. Furthermore, pathways involving more than five photons can be excluded as the error in the $\cos^{2n}\theta$ fit of the data doubles from its minimum at $n=3$ if $n>5$. This greatly reduces the number of combinations, allowing us to determine that the pathway producing the 2.3 eV KER peak is most likely the three-photon ATD, $a\,^4\Pi_u \rightarrow f\,^4\Pi_g - 3\omega$, pathway shown in Fig. 6(a) (the 2.3 eV is the sum of the 2.0 eV marked on the figure and the vibrational energy, as explained in Sec. III C 1). Other doublet and quartet pathways, such as $a\,^4\Pi_u \rightarrow f\,^4\Pi_g - 1\omega \rightarrow {}^4\Sigma_u^+ - 4\omega$ [see Fig. 6(b)], which produce the correct KER but the wrong angular distribution, fulfill some requirements, but only $a\,^4\Pi_u \rightarrow f\,^4\Pi_g - 3\omega$ fulfills *all* the necessary conditions.

2. Peak β

The most probable pathway leading to channel β will be determined using the same set of tools described above with the additional information gained by determining the pathway for α. Since channel β is predominant at a much lower intensity than channel α, one can assume that the pathway producing β requires a total emission and absorption of three or fewer photons, if the relevant transition matrix elements are comparable. Furthermore, all pathways starting from the $X\,^2\Pi_g$ state can be excluded, as pathways starting from this state that involve three or less photons will produce KER

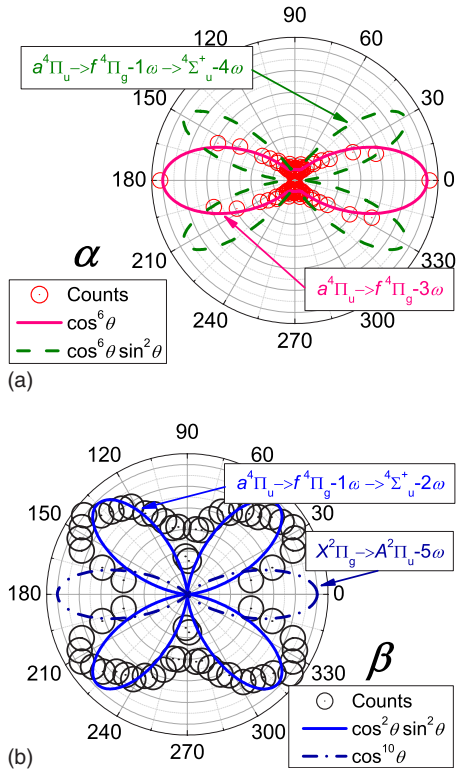

FIG. 5. (Color online) The measured angular distributions for two O_2^+ dissociation features. Panels (a) and (b) correspond to a range of KER values within peaks α and β, respectively. The size of the data symbols represents the error and data for $\theta > 180°$ is mirrored for display purposes. Fits corresponding to possible dissociation pathways described in the text are shown as lines. Note that with the aforementioned laser pulse, the molecule is predicted to rotate only slightly [24,45]. Therefore, we neglect the effect of these angular distortions here.

distributions peaked at zero as discussed earlier. Thus, the benchmark, channel α, and the selection rules have made the task of determining the pathway producing β much less arduous. Furthermore, the angular distribution, shown in Fig. 5(b), clearly indicates that the pathway must include both parallel and perpendicular transitions, as the distribution does not peak at 0° or 90°. These requirements and the axial-recoil approximation leave only one possible pathway, namely $a\,^4\Pi_u \rightarrow f\,^4\Pi_g - 1\omega \rightarrow {}^4\Sigma_u^+ - 2\omega$, which is analogous to a "double bond-softening" pathway as shown in Fig. 7(a). Again, other pathways, such as $X\,^2\Pi_g \rightarrow A\,^2\Pi_u - 5\omega$ shown in Fig. 7(b), will produce a KER distribution peaking around 1.5 eV; however, all will generate an angular distribution inconsistent with the data and require more photons than indicated by the intensity dependence of this feature.

C. Comparison with previous work

Though the main objective of this paper is to present the experimental method that allows us to identify the specific dissociation pathways in a many-electron molecule, it is interesting to compare the dissociation pathways we have identified with those previously found by Hishikawa *et al.* [27]. It is important to note that in their measurements the O_2 gas

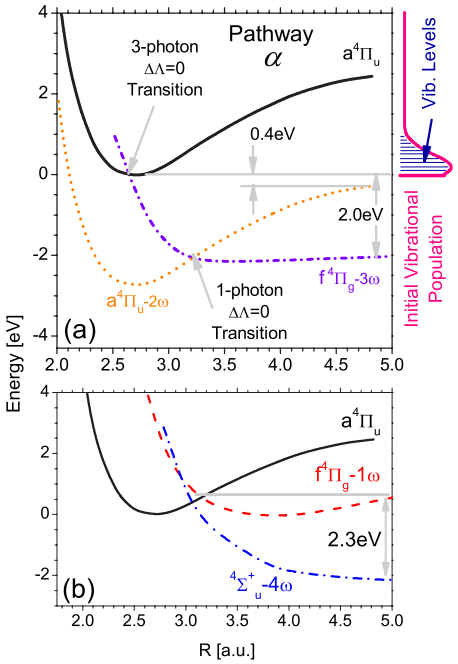

FIG. 6. (Color online) (a) The pathway for α and the approximate initial vibrational population of the $a\,^4\Pi_u$ state (see text). (b) A pathway leading to the measured KER peak for α, but failing to produce the observed angular dependence.

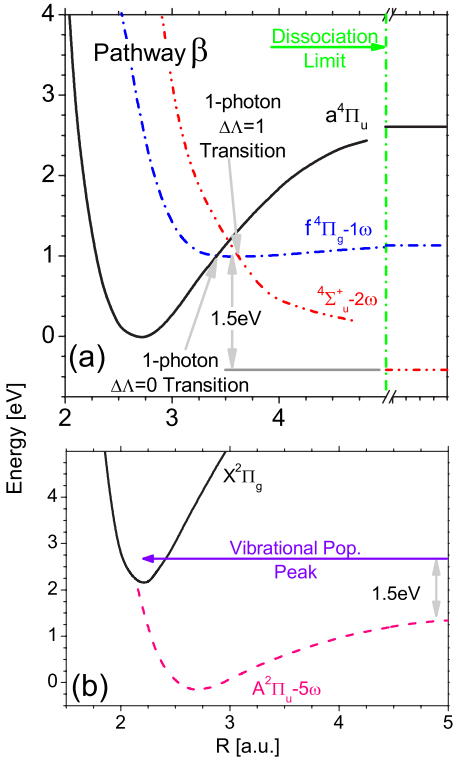

FIG. 7. (Color online) (a) The pathway for β as discussed in the text. (b) A pathway starting from the doublet ground state, $X\,^2\Pi_g$, which leads to the measured KER peak for β, but fails to produce the observed angular and intensity dependence.

target was first ionized, creating O_2^+, and subsequently dissociated by the same laser pulse. In contrast, in our measurements the ionization step is not necessary since the O_2^+ is generated by electron impact ionization. Therefore, some differences between the two measurements might be expected. The most noticeable difference is that in addition to features strongly aligned along the laser polarization such as those observed by Hishikawa *et al.* [27], we also observe dissociation pathways that involve perpendicular transitions, which result in an angular distribution that is not tightly aligned along the laser polarization. They identified two dissociation pathways of the $a\,^4\Pi_u$ state of O_2^+, which we will discuss below in further detail. Earlier work on the dissociation of O_2^+ [36,37] cannot be compared in detail because significantly shorter wavelengths were used. However, some of the KER structures observed in this work have similar features to those observed earlier.

Before comparing specific dissociation pathways to previous measurements, it is worth noting that the features we presented originate from the $a\,^4\Pi_u$ state and not from the $X\,^2\Pi_g$ O_2^+ ground state. In some previous studies, dissociative ionization through the $a\,^4\Pi_u$ state has been suggested to explain some observations [27,34]. In other studies, there was no indication for this intermediate state, and all the observations were consistent with ionization through the O_2^+ ground state [35–37].

1. Peak α

The first dissociation pathway, denoted as channel α above, involves a transition from the initial $a\,^4\Pi_u$ to the final $f\,^4\Pi_g - 3\omega$ state through the three-photon gap, as shown in Fig. 6(a). This dissociation pathway, identified also by Hishikawa *et al.* [27], yields a KER of about 2.0 eV for the $v=0$ state of $a\,^4\Pi_u$. (All vibrational levels bound in the PECs of interest were computed using the phase-amplitude method [57].) Higher vibrational states will also contribute, somewhat broadening and shifting the KER distribution to higher values, namely 2.3 eV with about 0.5 eV FWHM in our measurements. However, the yield of this path decreases rapidly with increasing v due to decreasing wave-function overlap (as is typical in this kind of curve crossing dynamics—predissociation is another example [58]) and consequent decrease in vibrational population, thus limiting the width of the KER peak for this process.

Note that, after making the $a\,^4\Pi_u \rightarrow f\,^4\Pi_g - 3\omega$ transition, the O_2^+ dissociating along this pathway can either (i) continue along the $f\,^4\Pi_g - 3\omega$ curve and dissociate as discussed above or (ii) cross to the $a\,^4\Pi_u - 2\omega$ state through a one-photon transition as indicated in Fig. 6(a). The dissociating O_2^+ reaches the $f\,^4\Pi_g - 3\omega \rightarrow a\,^4\Pi_u - 2\omega$ crossing ~ 10 fs after the three-photon transition has occurred. At this time the 40 fs FWHM laser pulse used in our measurements still provides strong one-photon coupling. Thus, a significant fraction of the dissociating wave packet is expected to make the transition to the $a\,^4\Pi_u - 2\omega$ final state yielding a smaller KER of about 0.4 eV for the $v=0$ state. This contribution should shift to higher KER values in a similar way as the α peak, thus resulting in about 0.7 eV (this feature is marked by a dashed arrow in Fig. 4). Both these KER features, namely a 2.3 eV peak from the $a\,^4\Pi_u \rightarrow f\,^4\Pi_g - 3\omega$ pathway and 0.7 eV peak from the $a\,^4\Pi_u \rightarrow f\,^4\Pi_g - 3\omega \rightarrow a\,^4\Pi_u - 2\omega$ pathway, appear in the highest intensity data shown in Figs. 3 and 4. Furthermore, the latter is more likely as expected. Note that the 0.7 eV peak appears also at lower intensities suggesting contributions of additional dissociation pathways, and therefore we cannot determine the branching ratio between these two pathways.

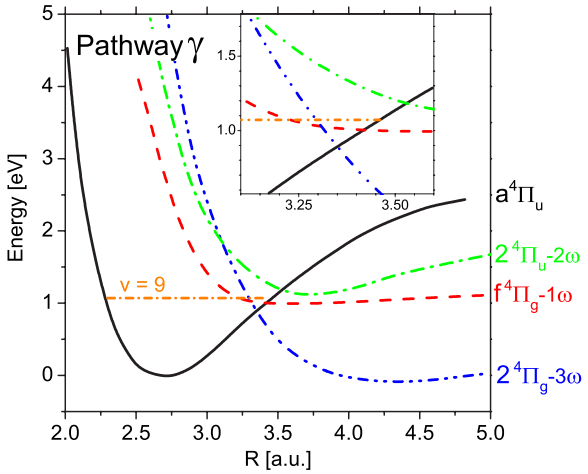

FIG. 8. (Color online) Pathway for γ as discussed in the text. The vibrational level nearest to the crossing is marked. The inset is an expanded view of the PEC crossings.

2. Peak γ

The second dissociation pathway suggested by Hishikawa *et al.* [27] involves a sequence of transitions though one-photon crossings, explicitly, $a\,^4\Pi_u \rightarrow f\,^4\Pi_g - 1\omega \rightarrow 2\,^4\Pi_u - 2\omega \rightarrow 2\,^4\Pi_g - 3\omega$, which yields a KER of about 0.8 eV. All these suggested crossings involve parallel transitions (i.e., Π to Π) and thus result in a strong angular alignment of the nuclear fragments along the laser polarization. Furthermore, this dissociation pathway is expected to be more efficient than the aforementioned three-photon pathway as it requires three one-photon couplings rather than a direct three photon transition, and thus it should occur even at lower intensities. This KER peak around 0.8 eV also appears in our data, but it vanishes at low intensities as can be seen in Figs. 3 and 4. Moreover, (i) this peak appears at the same intensity range as the peak labeled α, which is associated with a three-photon ATD dissociation pathway as discussed above, and (ii) it has a strongly aligned angular distribution. This suggests that a multiphoton mechanism of a similar order is involved, explicitly, the $a\,^4\Pi_u \rightarrow f\,^4\Pi_g - 1\omega \rightarrow 2\,^4\Pi_g - 3\omega$ dissociation pathway, which is shown in Fig. 8 and later referred to as 1+2-photon ATD because the second transition involves a two-photon coupling. The dissociation pathway suggested here will have the same KER distribution as the one suggested previously [27] because (i) it accesses the same vibrational population through the initial $a\,^4\Pi_u$ to $f\,^4\Pi_g - 1\omega$ crossing, which occurs around $v=9$, and (ii) it has the same $2\,^4\Pi_g - 3\omega$ dissociation limit. However, assuming dipole transition matrix elements of comparable magnitude,

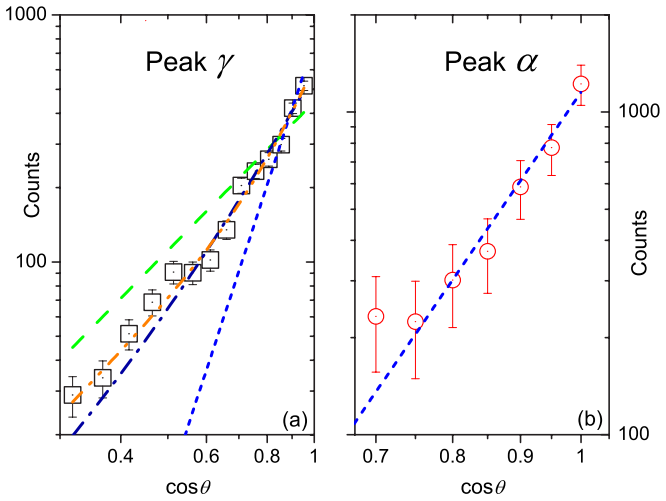

FIG. 9. (Color online) (a) and (b) Log-log plots of the measured yield (symbols) as a function of cos θ for the γ and α dissociation pathways, respectively. The lines shown in the figures are fits to the data of $N_0 \cos^6 \theta$ (short-dashed line), $N_0 \cos^2 \theta$ (long-dashed line), $N_0 \cos^2 \theta + N_1 \cos^4 \theta$ (dash-dot line), and $N_0 \cos^2 \theta + N_1 \cos^6 \theta$ (dash-dot-dot line). The last distribution fits the data in panel (a) best, but also the mixed $\cos^2 \theta + \cos^4 \theta$ distribution is consistent with the data as discussed in the text. The data in panel (b) nicely fit by a $\cos^6 \theta$ distribution.

the current pathway will occur only at intensities higher than the previously suggested pathway due to the two-photon transition. This example demonstrates the impact of the intensity difference method on one's ability to determine the correct dissociation pathway.

It is also notable that the γ peak in Fig. 4 seems to sit on top of a wider KER distribution, which is visible at the lower intensities shown in the figure. This broad energy tail is most likely due to the $a\,^4\Pi_u \rightarrow f\,^4\Pi_g - 1\omega$ dissociation shown in Fig. 8, which produces a KER distribution similar to the one shown in Fig. 2(b) because the crossing is below the dissociation limit. This parallel one-photon transition, typically referred to as bond softening [10,11] is expected to yield a $\cos^2 \theta$ angular distribution. Furthermore, we cannot totally exclude contributions from the dissociation of highly excited vibrational states of the $X\,^2\Pi_g$ ground state of O_2^+ through the crossing with the $A\,^2\Pi_u - 1\omega$ state, which is also expected to yield a $\cos^2 \theta$ angular distribution. However, the population of such highly excited vibrational states ($v \gtrsim 30$) is expected to be negligible. Due to this KER tail, the angular distribution of the γ peak is a mixture of a $\cos^2 \theta$ distribution from the aforementioned one-photon process and a $\cos^6 \theta$ distribution from the 1+2-photon ATD discussed above. This angular distribution nicely fits the data as shown in Fig. 9. However, the data is also consistent with a mixed $\cos^2 \theta + \cos^4 \theta$ distribution illustrating the difficulty in eliminating possible pathways based only on their angular distribution. Nevertheless, we have not found a two-photon pathway which involves only parallel transitions and yields 0.8 eV, thus we conclude that the pathway we suggest above is the most likely one.

3. Peak β

The dissociation pathway denoted as channel β above has a wider angular distribution and peaks at a KER of ~1.5 eV. We identified the dissociation pathway to be a sequence of two one-photon transitions, namely $a\,^4\Pi_u \rightarrow f\,^4\Pi_g - 1\omega \rightarrow {}^4\Sigma_u^+ - 2\omega$ as explained earlier. It is important to note that this dissociation pathway appears at lower laser intensities than the previous two pathways as expected for the lower number of photons involved in these transitions. Furthermore, this dissociation pathway involves similar vibrational states of the $a\,^4\Pi_u$ electronic state as the three-photon ATD pathway to the $2\,^4\Pi_g - 3\omega$ state, namely $v \sim 7-9$. More importantly, this dissociation pathway, which dominates our low intensity spectra, was not observed previously [27], most likely because the need to first ionize the neutral oxygen target sets a limit on the lowest intensities at which one can study O_2^+ dissociation.

IV. CONCLUSION

In summary, using the intensity dependence, the shape and position of the KER peak, the angular distribution, and the dipole selection rules, one can determine the most probable laser-induced dissociation pathway(s) for a feature that has a distinct dissociation momentum distribution. Furthermore, once the pathway leading to a particular feature is determined, it can be used as an intensity benchmark to set the upper or lower limit of photons required along another pathway of interest. This method can be extended to other features in the KER-cos θ distribution of O_2^+ and is expected to work for any diatomic molecule in a laser field that is measured with a complete 3D intensity-dependent momentum imaging technique. It is important to note that in order to apply this method a few assumptions need to be valid, namely (i) the axial-recoil approximation, (ii) dipole transition matrix elements for the relevant allowed transitions are of comparable magnitude, and (iii) the conditions allowing the use of the IDS method [52].

Employing this method, we have investigated a few of the O_2^+ dissociation pathways in an intense 40 fs laser pulse and identified them as (i) α — a three-photon ATD pathway strongly aligned along the laser polarization occurring predominantly at intensities above 6×10^{14} W/cm^2, (ii) β — a dissociation channel involving two one-photon transitions, one parallel and one perpendicular, that happens mainly at lower intensities below about 10^{14} W/cm^2, and (iii) γ — a 1+2-photon ATD pathway occurring at similar intensities as α. All of these are dissociation pathways of the $a^4\Pi$ metastable state of O_2^+.

ACKNOWLEDGMENTS

We wish to thank Professor Zenghu Chang's group for providing the laser beam and C. Fehrenbach for technical help. This work was supported by the Chemical Sciences, Geosciences, and Biosciences Division, Office of Basic Energy Sciences, Office of Science, U.S. Department of Energy.

[1] A. Giusti-Suzor, F. H. Mies, L. F. DiMauro, E. Charron, and B. Yang, J. Phys. B **28**, 309 (1995).
[2] A. Zavriyev, P. H. Bucksbaum, H. G. Muller, and D. W. Schumacher, Phys. Rev. A **42**, 5500 (1990).
[3] A. Rudenko, B. Feuerstein, K. Zrost, V. L. B. de Jesus, T. Ergler, C. Dimopoulou, C. D. Schröter, R. Moshammer, and J. Ullrich, J. Phys. B **38**, 487 (2005).
[4] J. Ludwig, H. Rottke, and W. Sandner, Phys. Rev. A **56**, 2168 (1997).
[5] V. N. Serov, A. Keller, O. Atabek, and N. Billy, Phys. Rev. A **68**, 053401 (2003).
[6] P. H. Bucksbaum, A. Zavriyev, H. G. Muller, and D. W. Schumacher, Phys. Rev. Lett. **64**, 1883 (1990).
[7] A. D. Bandrauk and M. L. Sink, J. Chem. Phys. **74**, 1110 (1981).
[8] A. Giusti-Suzor, X. He, O. Atabek, and F. H. Mies, Phys. Rev. Lett. **64**, 515 (1990).
[9] J. H. Posthumus, Rep. Prog. Phys. **67**, 623 (2004).
[10] A. Zavriyev, P. H. Bucksbaum, J. Squier, and F. Saline, Phys. Rev. Lett. **70**, 1077 (1993).
[11] P. H. Bucksbaum, A. Zavriyev, H. G. Muller, and D. W. Schumacher, Phys. Rev. Lett. **64**, 1883 (1990).
[12] Th. Ergler, A. Rudenko, B. Feuerstein, K. Zrost, C. D. Schröter, R. Moshammer, and J. Ullrich, Phys. Rev. Lett. **95**, 093001 (2005).
[13] D. Normand, C. Cornaggia, and J. Morellec, J. Phys. B **19**, 2881 (1986).
[14] A. Saenz, Phys. Rev. A **66**, 063408 (2002).
[15] Th. Ergler, A. Rudenko, B. Feuerstein, K. Zrost, C. D. Schröter, R. Moshammer, and J. Ullrich, Phys. Rev. Lett. **97**, 193001 (2006).
[16] B. Yang, M. Saeed, L. F. DiMauro, A. Zavriyev, and P. H. Bucksbaum, Phys. Rev. A **44**, R1458 (1991).
[17] C. Cornaggia, D. Normand, J. Morellec, G. Mainfray, and C. Manus, Phys. Rev. A **34**, 207 (1986).
[18] S. Chelkowski, A. Conjusteau, T. Zuo, and A. D. Bandrauk, Phys. Rev. A **54**, 3235 (1996).
[19] Th. Ergler, A. Rudenko, K. Zrost, C. D. Schröter, R. Moshammer, and J. Ullrich, J. Phys. B **39**, S493 (2006).
[20] T. Zuo and A. D. Bandrauk, Phys. Rev. A **52**, R2511 (1995).
[21] T. D. G. Walsh, F. A. Ilkov, S. L. Chin, F. Châteauneuf, T. T. Nguyen-Dang, S. Chelkowski, A. D. Bandrauk, and O. Atabek, Phys. Rev. A **58**, 3922 (1998).
[22] R. Numico, A. Keller, and O. Atabek, Phys. Rev. A **56**, 772 (1997).
[23] I. Kawata, H. Kono, and Y. Fujimura, J. Chem. Phys. **110**, 11152 (1999).
[24] M. Uhlmann, T. Kunert, and R. Schmidt, Phys. Rev. A **72**, 045402 (2005).
[25] H. Niikura, F. Légaré, R. Hasbani, A. D. Bandrauk, M. Yu. Ivanov, D. M. Villeneuve, and P. B. Corkum, Nature (London) **417**, 917 (2002).
[26] M. F. Kling, Ch. Siedschlag, A. J. Verhoef, J. I. Khan, M. Schultze, Th. Uphues, Y. Ni, M. Uiberacker, M. Drescher, F. Krausz, and M. J. J. Vrakking, Science **312**, 246 (2006).
[27] A. Hishikawa, S. Liu, A. Iwasaki, and K. Yamanouchi, J. Chem. Phys. **114**, 9856 (2001).
[28] A. S. Alnaser, S. Voss, X. M. Tong, C. M. Maharjan, P. Ranitovic, B. Ulrich, T. Osipov, B. Shan, Z. Chang, and C. L. Cocke, Phys. Rev. Lett. **93**, 113003 (2004).
[29] C. M. Marian, R. Marian, and S. D. Peyerimhoff, Mol. Phys. **46**, 779 (1982).
[30] A. Assion, T. Baumert, U. Weichmann, and G. Gerber, Phys. Rev. Lett. **86**, 5695 (2001).
[31] M. Machholm and A. Suzor-Weiner, J. Chem. Phys. **105**, 971 (1996).
[32] K. Codling and L. J. Frasinski, J. Phys. B **26**, 783 (1993).
[33] C. Cornaggia and L. Quaglia, Phys. Rev. A **63**, 030702(R) (2001).
[34] B. L. J. Bakker and D. H. Parker, J. Chem. Phys. **112**, 4037 (2000).
[35] B. L. J. Bakker, D. H. Parker, P. C. Samartzis, and T. N. Kitsopoulos, J. Chem. Phys. **112**, 5654 (2000).
[36] C. Cornaggia, J. Lavancier, D. Normand, J. Morellec, P. Agostini, J. P. Chambaret, and A. Antonetti, Phys. Rev. A **44**, 4499 (1991).
[37] D. Normand, C. Cornaggia, J. Lavancier, J. Morellec, and H. X. Liu, Phys. Rev. A **44**, 475 (1991).
[38] L. Quaglia, O. Chiappa, G. Granucci, V. Brenner, Ph. Millié, and C. Cornaggia, J. Phys. B **35**, L145 (2002).
[39] C. Guo, M. Li, and G. N. Gibson, Phys. Rev. Lett. **82**, 2492 (1999).
[40] C. Guo, M. Li, J. P. Nibarger, and G. N. Gibson, Phys. Rev. A **61**, 033413 (2000).
[41] X. M. Tong, Z. X. Zhao, and C. D. Lin, Phys. Rev. A **66**, 033402 (2002).
[42] S. Voss, A. S. Alnaser, X. M. Tong, C. Maharjan, P. Ranitovic, B. Ulrich, B. Shan, Z. Chang, C. D. Lin, and C. L. Cocke, J. Phys. B **37**, 4239 (2004).
[43] A. S. Alnaser, M. Zamkov, X. M. Tong, C. M. Maharjan, P. Ranitovic, C. L. Cocke, and I. V. Litvinyuk, Phys. Rev. A **72**, 041402(R) (2005).
[44] B. Walker, M. Saeed, T. Breeden, B. Yang, and L. F. DiMauro, Phys. Rev. A **44**, 4493 (1991).
[45] X. M. Tong, Z. X. Zhao, A. S. Alnaser, S. Voss, C. L. Cocke, and C. D. Lin, J. Phys. B **38**, 333 (2005).
[46] A. Tabché-Fouhaillé, J. Durup, J. T. Moseley, J. B. Ozenne, C. Pernot, and M. Tadjeddine, Chem. Phys. **17**, 81 (1976).
[47] Z. Amitay, A. Baer, M. Dahan, J. Levin, Z. Vager, D. Zajfman, L. Knoll, M. Lange, D. Schwalm, R. Wester, A. Wolf, I. F. Schneider and A. Suzor-Weiner, Phys. Rev. A **60**, 3769 (1999).
[48] W. J. van Der Zande, W. Koot, J. R. Peterson, and J. Los, Chem. Phys. **126**, 169 (1988).
[49] I. Ben-Itzhak, P. Q. Wang, J. F. Xia, A. M. Sayler, M. A. Smith, K. D. Carnes, and B. D. Esry, Phys. Rev. Lett. **95**, 073002 (2005).
[50] P. Q. Wang, A. M. Sayler, K. D. Carnes, J. F. Xia, M. A. Smith, B. D. Esry, and I. Ben-Itzhak, Phys. Rev. A **74**, 043411 (2006).
[51] I. Ben-Itzhak, P. Q. Wang, J. F. Xia, A. M. Sayler, M. A. Smith, J. W. Maseberg, K. D. Carnes, and B. D. Esry, Nucl. Instrum. Methods Phys. Res. B **233**, 56 (2005).
[52] P. Q. Wang, A. M. Sayler, K. D. Carnes, B. D. Esry, and I. Ben-Itzhak, Opt. Lett. **30**, 664 (2005).
[53] In our experiment, the molecular ion beam thickness (0.7 ± 0.05 mm) is much thinner than the laser's confocal parameter (3.4 ± 0.2 mm), and the laser focal spot diameter (45 ± 4 μm FWHM) is much smaller than the molecular ion beam width (0.7 ± 0.05 mm).

[54] M. Plummer and J. F. McCann, J. Phys. B **30**, L401 (1997).
[55] Liang-You Peng, I. D. Williams, and J. F. McCann, J. Phys. B **38**, 1727 (2005).
[56] The separation between adjacent vibrational levels in O_2^+ is <0.25 eV. Thus, features separated by $\gtrsim 0.5$ eV are assumed to be due to O_2^+ electronic structure.
[57] Emil Y. Sidky and Itzik Ben-Itzhak, Phys. Rev. A **60**, 3586 (1999).
[58] A. D. Bandrauk and M. L. Sink, J. Chem. Phys. **74**, 1110 (1981).